iScience

CellPress
OPEN ACCESS

Article

The forbidden band and size selectivity of acoustic radiation force trapping

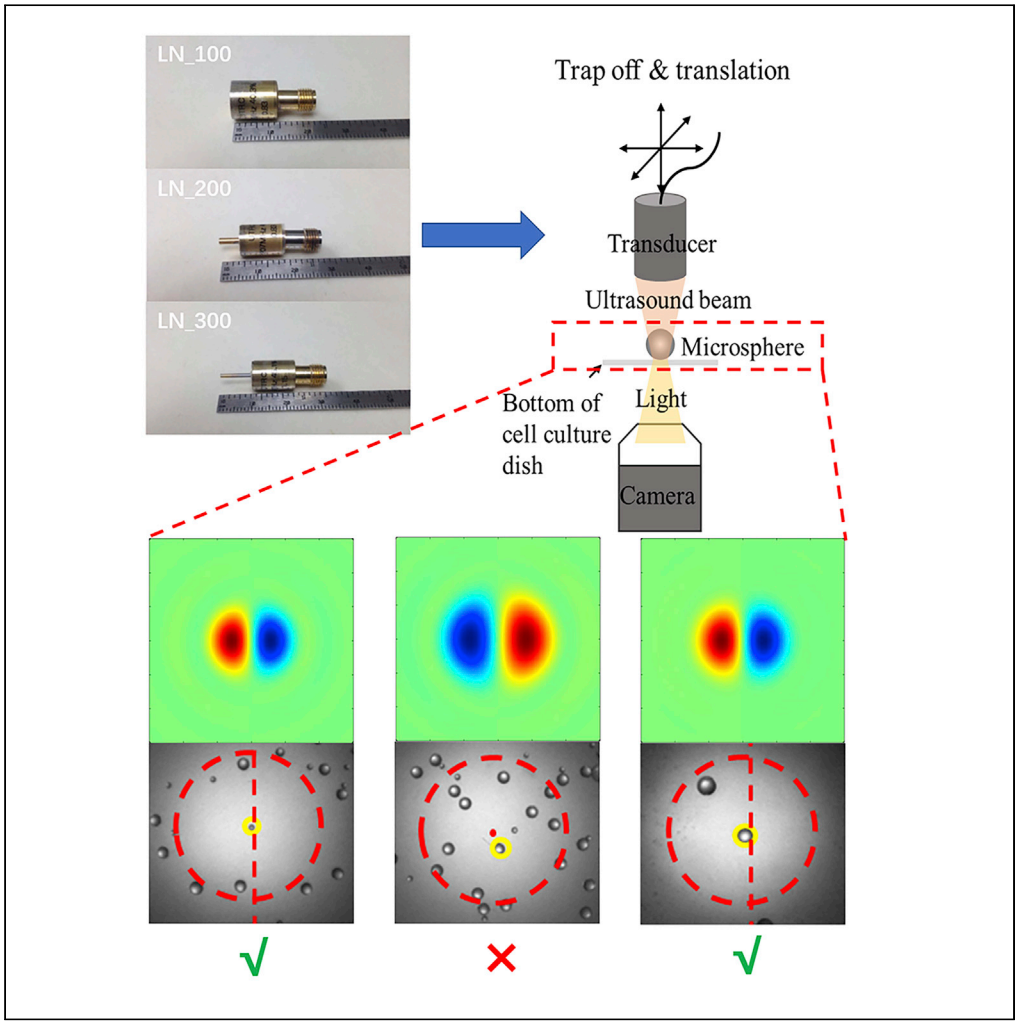

Zhaoxi Li, Danfeng Wang, Chunlong Fei, ..., Zeyu Chen, Wei Feng, Yintang Yang

clfei@xidian.edu.cn (C.F.)
ytyang@xidian.edu.cn (Y.Y.)

HIGHLIGHTS

Ultrahigh-frequency (≥100 MHz) ultrasonic transducer to manipulate microspheres

The broad bandwidth and highly focused transducer differentiate microparticles

FEA modeling and calculation indicate the force for selectively trapping

The forbidden band theory of acoustic radiation force is proposed for trapping

Li et al., iScience *24*, 101988
January 22, 2021
https://doi.org/10.1016/j.isci.2020.101988

iScience

CellPress
OPEN ACCESS

Article

The forbidden band and size selectivity of acoustic radiation force trapping

Zhaoxi Li,[1,5] Danfeng Wang,[2,5] Chunlong Fei,[1,4,6,*] Zhihai Qiu,[3] Chenxue Hou,[1] Runcong Wu,[1] Di Li,[1] Qidong Zhang,[1] Dongdong Chen,[1] Zeyu Chen,[2] Wei Feng,[4] and Yintang Yang[1,*]

SUMMARY

Acoustic micro-beams produced by highly focused ultrasound transducer have been investigated for micro-particle and cell manipulation. Here we report the selective trapping of microspheres via the acoustic force using the single acoustical beam. The forbidden band theory of acoustic radiation force trapping is proposed, which indicates that the trapping of particles via the acoustic beam is directly related to the particle diameter-to-beam wavelength ratio as well as excitation frequency of the ultrasonic acoustic tweezers. Three tightly focused $LiNbO_3$ transducers with different center frequencies were fabricated for use as selective single beam acoustic tweezers (SBATs). These SBATs were capable of selectively manipulating microspheres of sizes 5–45 μm by adjusting the wavelength of acoustic beam. Our observations could introduce new avenues for research in biology and biophysics by promoting the development of a tool for selectively manipulating microspheres or cells of certain selected sizes, by carefully setting the acoustic beam shape and wavelength.

INTRODUCTION

Particle manipulation by a contactless method has numerous applications in biophysical and biomedical research areas (Lam et al., 2012; Tomasi et al., 2020; Yu and Miyako, 2018; Diamantaki et al., 2018; Patnode et al., 2019; Ozcelik et al., 2018; Melde et al., 2016). Optical tweezer is an outstanding example capable of trapping and manipulating various types of microparticles (Yu and Miyako, 2018; Maragò et al., 2013; Ashkin et al., 1986; Grier, 2003; Kotamarthi et al., 2020). It has been utilized to measure the elastic properties of the DNA molecular chain (Fazal and Block, 2011), rotate the microspheres or cells in many fields (Padgett and Bowman, 2011), and assemble 1D, 2D, and 3D array structures of embryonic stem cells (Kirkham et al., 2015). However, the focused lasers used to realize optical tweezers could cause local heating and photodamage in biological samples because of the high energy it generates. In addition, the applied force by optical tweezer is small, of the order of ~pN or ~ fN (Quinto-Su, 2014; Keloth et al., 2018). These problems can be avoided by using acoustic tweezers because acoustic energy is unlikely to damage biological samples (Neuman and Nagy, 2008; Choe et al., 2011; Liu and Hu, 2009; Marston, 2006; Wu, 1991). Moreover, these acoustic instruments are not only much easier to set up but also incur lower costs than their optical counterparts.

Recently, single beam acoustic tweezers (SBATs), analogous to optical tweezers for trapping and manipulating the individual particle with an acoustic micro-beam (Lee et al., 2005, 2009; Lee and Shung, 2006; Zhu et al., 2016; , (Baudoin et al., 2020b); Kamsma et al., 2018; Sitters et al., 2014) have attracted considerable attention. Over the past decade, acoustic trapping using SBATs has been investigated both theoretically and experimentally. Owing to the advances of high-frequency ultrasound transducer fabrication process, the performance of acoustic tweezers has been considerably improved over time. Transducers capable of operating at 200 MHz have also been developed, and are shown in Figure 1A, which has enabled the trapping of cells with sizes 15–20 μm (Lee et al., 2011), as well as microspheres with diameters 5 and 10 μm (Marston, 2006).

The performance of acoustic trapping with SBATs is influenced by various factors, including the acoustic characteristics of the medium, excitation frequency of the transducer, distribution of the acoustic field,

[1]School of Microelectronics, Xidian University, Xi'an, China

[2]School of Mechanical and Electrical Engineering, Central South University, Changsha, China

[3]Department of Radiology, Stanford University, Stanford, CA, USA

[4]Shenzhen Institutes of Advanced Technology, Chinese Academy of Sciences, Shenzhen 518055, China

[5]These authors contributed equally

[6]Lead contact

*Correspondence: clfei@xidian.edu.cn (C.F.), ytyang@xidian.edu.cn (Y.Y.)

https://doi.org/10.1016/j.isci.2020.101988

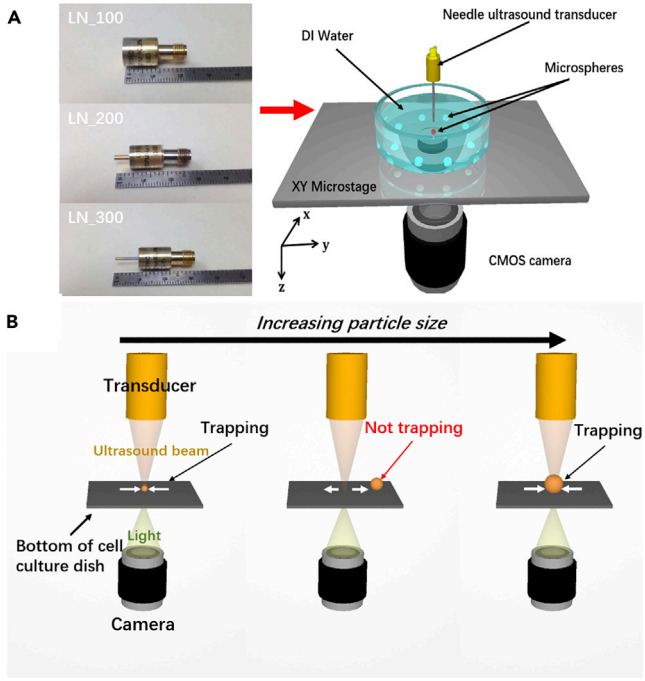

Figure 1. Schematic diagram of the experimental setup and principle

(A and B) Particle trapping using single beam acoustic tweezer (SBAT, A) and size-selective trapping (B).

and the size, shape, and material properties of the particles themselves. In general, the smaller the particles that are needed to be trapped, the higher the SBAT frequency must be. These provide a simple logic for selecting and differentiating the trapping object by its size range from 5 to 50 μm by tuning the frequency used from 100 to 300 MHz. Besides the well-known influence of size-to-wavelength, we propose the "forbidden band" of acoustic trapping. Thus, trapping of particles whose diameters are in the range of the acoustic wavelength is not possible due to the positive gradient of acoustic radiation force (ARF). Figure 1B shows the schematic diagram of the size-selectivity manipulation of single microspheres of different sizes.

However, several problems still need to be addressed to realize trapping microsphere using transducers. First, it is difficult for a typical SBAT to achieve a -6 dB bandwidth of more than 30%, which means that the frequency range in which the transducer can be excited is small, and thus the range of particle sizes to trap using the SBAT is limited. Nevertheless, the broad bandwidth and highly focused transducers for SBAT applications are quite challenging to manufacture, particularly of one operating in the ultrahigh frequency range (>100 MHz). In addition, the SBAT needs to show characteristic features, e.g., a low f-number and a cylindrical symmetry of the acoustic beam, to meet the requirements of biomedical and biological applications (see Figure S1 and Table S1 in Supplemental information for detailed definition of these parameters).

Based on our prior work, size-selective manipulation of single particles in the range 3–100 μm can be achieved with frequencies between 150 and 400 MHz (Chen et al., 2017). However, the range of the trapping was successful or failed using the different ultrahigh frequency ultrasonic transducers with different f-number has not been previously reported, and it is very important to explain and quantify the trapping ability of the focusing transducers with different characterization for the various the acoustic contrast between microspheres or cells and medium, which would be of significant importance both in research and industrial applications.

In this work, we combined experimental and theoretical investigations to give the phenomenon and explanation of size selectivity of acoustic radiation force trapping via the highly focused transducers. Three high-performance (with low f-number and broad bandwidth) ultrahigh frequency ultrasound transducers are

designed and fabricated for generating tightly focused ultrasound beam. We find that there is a grabbing band corresponding to size of the microparticle and ultrasound frequency within a certain range. The forbidden band is given by calculation of acoustic radiation force for microsphere and verified by experiment. This platform can be used to manipulate and differentiate specific microparticles without disturbing other particles.

RESULTS

Characteristic of acoustic field by three highly focused transducers with different center frequencies

To realize individual particle mobilization of elastic micro-particles suspended in liquids, the ultrasound beam width of single-beam acoustic tweezers should be close to the particle size with a highly focused ultrasonic beam that can produce sufficient specific force for trapping and manipulating a micro-particle of interest.

Tightly focused $LiNbO_3$ transducers (LN100, LN200, and LN300) with center frequency around 100 MHz, 200 MHz, and 300 MHz were evaluated and used to trap microspheres of 5–15 μm at their focus. All the transducers show high sensitivity and relatively broad −6 dB bandwidth. The ultrahigh center frequency, broad bandwidth, high sensitivity, and small $f_{\#}$ make the transducers suitable for SBAT applications. The receive-echo response, corresponding frequency spectrum, as well as the lateral beam profile of the $LiNbO_3$ focused transducers are shown in Figure S1, and a beam width equal to 16.4, 6.6, and 6.4 μm was obtained by transducers "LN_100", "LN_200," and "LN_300," respectively, in detecting a spatial point target at full width at half maximum (FWHM, −6 dB). The schematic structure of the transducers is shown in Figure 2A; these transducers have $f_{\#}$ values close to 1.0 with the theoretical values for the beam width of −6 dB lateral beam being 12.4, 6.4, and 6.2 μm (= $f_{\#}$ × wavelength) for LN_100, LN_200, and LN_300 at 104, 207, and 275 MHz in water (sound velocity is 1,540 m/s), respectively (see Table S1).

The map of acoustics pressure was achieved using finite element method (FEM) in the COMSOL environment. The COMSOL model is constructed in a two-dimensional axisymmetric coordinate system, and the plane wave radiation is set at the boundary of the propagation medium. Here, we focus on the case of the LN_200 transducer, and the aperture size of the piezoelectric element is 0.8 × 0.8 mm^2 with the measured center frequency of 207 MHz and the −6 dB bandwidth of 44.2%. In the FEM, the ultrahigh frequency focused LN_200 transducer with a piezoelectric layer (15 μm) and its matching layer (2.5 μm) in the form of double-layer rings are attached to the hemispherical water area (1.2 mm diameter) and focal plane at z = 0. The maximum calculation grid size of water area is set to one-fifth wavelength in the water at excitation frequency. The LN_200 transducer is operated at a frequency of 200–300 MHz corresponding to a wavelength of 7.7–5.1 μm in water. The acoustic pressure waveforms were simulated at each point in a hemisphere and a rectangle on the xz plane in increments of λ/15 for different frequencies and quarter circles. Moreover, the principle setup and the model parameters (2D-axisymmetric coordinate system, boundary conditions, relative resolution) are the same for all three transducers. A cross-section of the computational model and calculated results for the acoustic field, e.g., magnitude and phase of acoustic pressure as well as the angular spectrum, are shown in Figure 2. Based on these results, it can be observed that beam focusing is achieved almost at the focal position (z = 0 mm) of the needle transducer, while the lateral −6 dB beam width of the pressure amplitude at the focal point is 6.56 μm in Figure 2G, which is in agreement with the theoretical value (6.2 μm) based on f-number and wavelength.

Using the finite element analysis software, the aforementioned three tightly focused transducers (LN_100, LN_200, and LN_300) were modeled and simulated (see Figure S2), and the simulated -6 dB lateral beam widths of 17.9, 7.0, and 6.7 μm agree with the experimental value of 16.4, 6.4, and 6.2 μm at central frequency. Sound field distribution and lateral beam characteristics at the focus of the three transducers are given in the Figure S3.

Acoustic radiation force of ultrasonic transducer

The lateral component of the radiation force determines whether the particles can be manipulated to move them in the lateral direction; owing to the symmetry of the acoustic field, only a certain direction needs to be considered. Then, the acoustic radiation forces on the microspheres can be calculated as

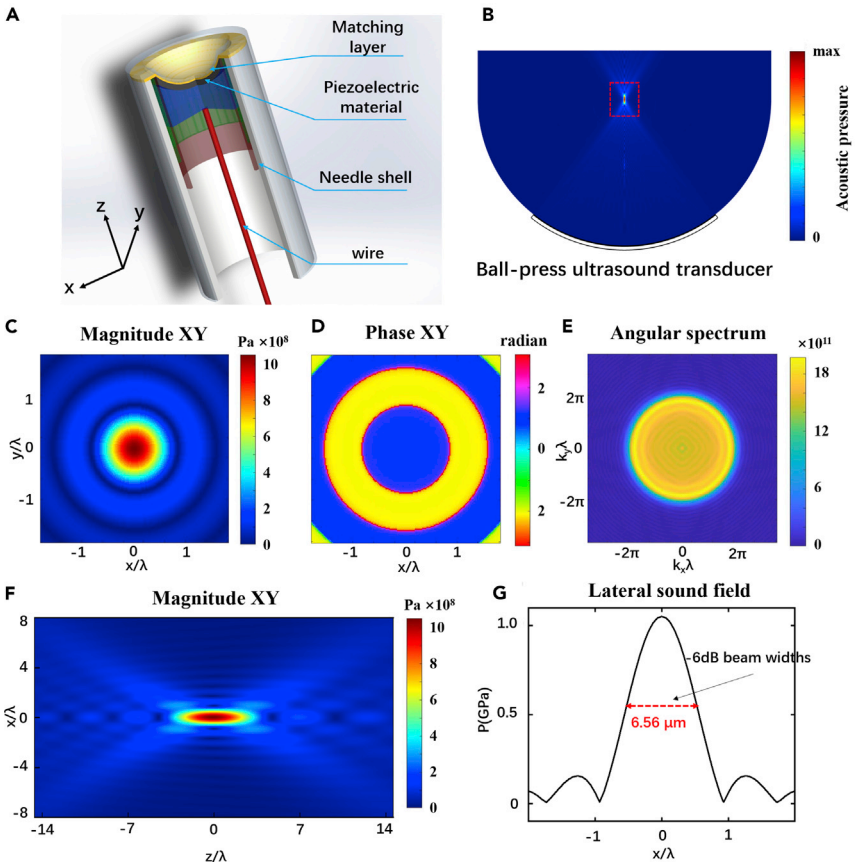

Figure 2. Schematic setup and characterization of focused ultrasound transducer

(A–G) The focused transducer was fabricated using the ball-press technique (A) and 2D model used for FEM simulations (B, see Figure S2 in Supplemental information for details). Acoustic pressure field emitted by the LN_200 transducer (200-MHz nominal center frequency) evaluated in the focal plane (z = 0) at frequency 250 MHz (C–G): magnitude (C), phase (D), and absolute value of angular spectrum (E). Cross-sectional view (xz) of magnitude (F) in the focal region (red-dotted box in B) as well as beam profile for y = 0 (G) with -6 dB beam width indicated by red line.

detailed in Transparent Methods. The spherical scatterer (polystyrene microsphere) and the medium (water) are used in calculation with the following parameters: ρ = 1,000 kg/m^3, c = 1,540 m/s, ρ_s = 1,040 kg/m^3, c_l = 2,330 m/s, and c_t = 1,100 m/s. The lateral component of the acoustic radiation force Fx was calculated (based on Equations S3–S9 in Transparent methods) for different particles sizes (5–15 μm) and for frequencies between 200 and 300 MHz. Their distribution at 250 MHz was plotted; these results are shown in Figure 3, and these parameters correspond to size-to-wavelength ratios from 0.8 to 2.4. Qualitative different behavior of the radiation force can be observed depending on the particle size. For particles with 5 μm (Figures 3A) and 15 μm (Figure 3C) diameter the radiation force is directed toward the center of the acoustic beam (x = 0). This attractive force allows for particle trapping even if the transducer is slightly moved in the lateral direction. In contrast to this, radiation force acting on the 10-μm particle is directed away from the acoustic beam axis pushing the particle off the focal area. These calculations indicate that the manipulation of particles of different sizes using the transducer produces two different behaviors, namely, pulling back or pushing away, leading to selective trapping.

Criteria of selective trapping

The capability of $LiNbO_3$ ultrahigh frequency microbeam devices for size-selective trapping of a single microsphere was demonstrated via calculation of the acoustic force at 250 MHz with the LN_200 transducer. To further understand the selective trapping of particles, we repeated the simulation of the distribution of acoustic pressure produced by the transducer using FEM and the calculation of acoustic force for microspheres with different radii for three different ultrasound

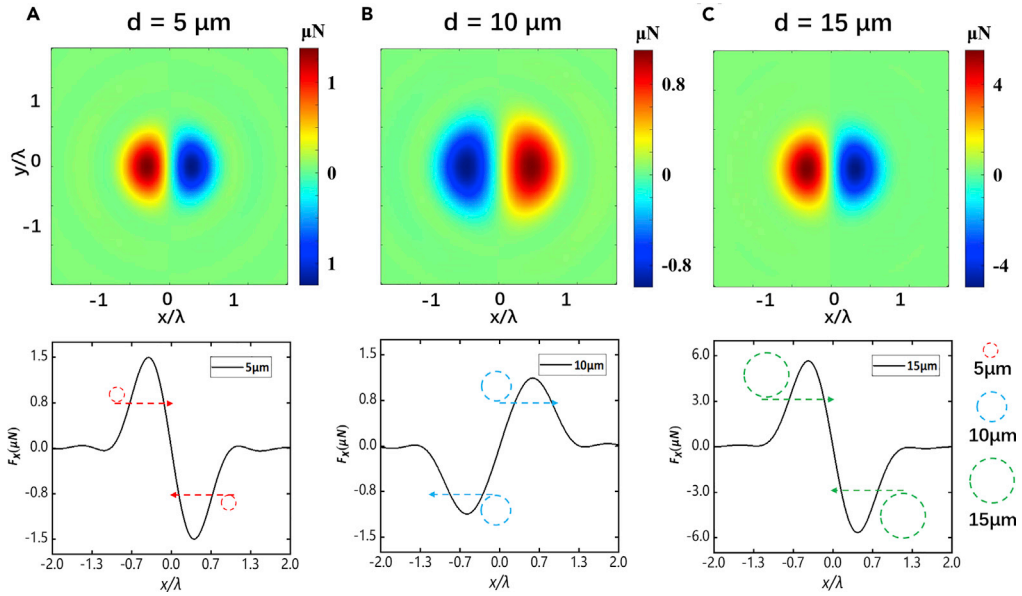

Figure 3. Calculation of acoustic radiation forces

The diameters of the three different scatterers are 5 μm (A), 10 μm (B) and 15 μm (C).Lateral distributions (top) of the lateral component of force Fx on the xy plane for different diameters d of the scatterer (microsphere) calculated based on angular spectrum decomposition at 250 MHz, and plots for acoustic radiation forces Fx along the y = 0 line (bottom) in the force map shown on top; red, blue, and green dotted circles represent scatterers of different sizes as indicated in the figure.

transducers at different frequencies. To better scan and get the corresponding relationship diagram, the result F_x of the abovementioned formula is taken as the corresponding one-dimensional drawing group in the middle axial direction ($F_{x,y=0}$). Supposing there are two cases of the microsphere under the focus beam (can trap or cannot trap), these two cases can be defined by the following discriminant:

$$\left.\frac{dF_{x,y=0}}{dx}\right|_{x=0} > 0 \quad or \quad \left.\frac{dF_{x,y=0}}{dx}\right|_{x=0} < 0 \ ? \qquad \text{(Equation 1)}$$

$$\left.\frac{dF_{x,y=0}}{dx}\right|_{x=0} = \frac{C * Re\left\{\sum_{n=0}^{\infty}\psi_n\sum_{m=-n}^{n}A_{nm}\left(\Delta H_{nm}\Delta H^*_{n+1,m+1} - \Delta H_{n,-m}\Delta H^*_{n+1,-m-1}\right)\right\}}{x_s} \qquad \text{(Equation 2)}$$

$$\Delta H_{nm} = \int\int_{k_x^2+k_y^2\le k^2}\left(e^{ik_x x_s}-1\right)dk_x dk_y S(k_x,k_y)Y^*_{nm}(\theta_k,\phi_k)$$

where the C is $1/(8\pi^2\,\rho c^2\,k^2)$ and x_s is defined as the size of the calculation grid (1/20λ) in the x direction in FEM. When $\left.\frac{dF_{x,y=0}}{dx}\right|_{x=0} > 0$, as described in Figure 3B, the corresponding microsphere will move away from the focus beam center. Otherwise, Figures 3A and 3C conform to the condition of $\left.\frac{dF_{x,y=0}}{dx}\right|_{x=0} < 0$ and the microsphere will be trapped at the center by acoustic radiation force. The discriminating factor $\left.\frac{dF_{x,y=0}}{dx}\right|_{x=0}$ values as a function of d and frequency of the three focused transducers are all calculated as shown in Figure 4(A1–C1). With the change of the size of the microsphere (d) and the excitation frequency (f), the three transducers all show the "Forbidden band" in which the discriminating factor becomes positive and meets the condition of $\left.\frac{dF_{x,y=0}}{dx}\right|_{x=0} > 0$. To characterize the band gap more clearly, both $\left.\frac{dF_{x,y=0}}{dx}\right|_{x=0}$ are depicted in the gray scale diagram and the x coordinates are normalized to d/lambda, as shown in Figure 4, which set the A is $\left.\frac{dF_{x,y=0}}{dx}\right|_{x=0} > 0$ and B is $\left.\frac{dF_{x,y=0}}{dx}\right|_{x=0} < 0$. When given a transducer ($f_\#$ and DOF),

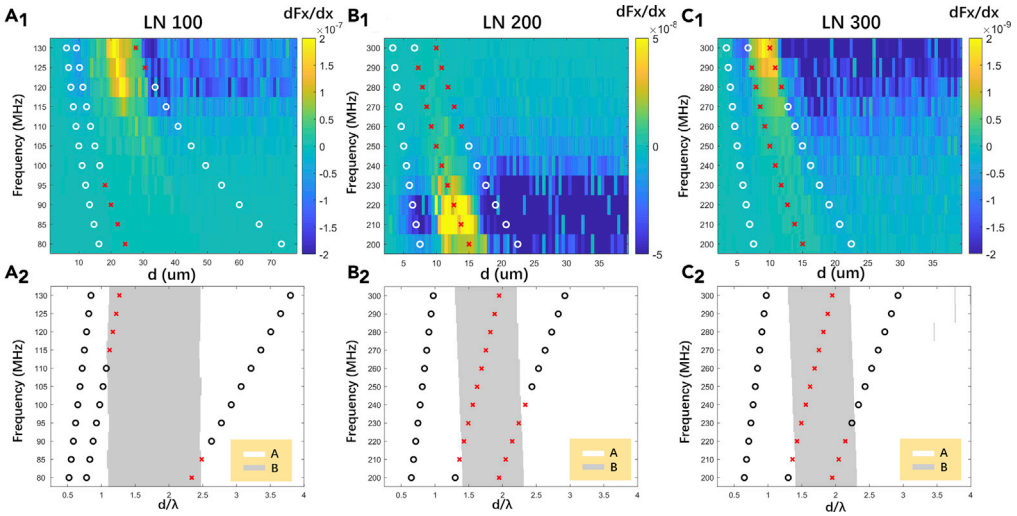

Figure 4. Dependence of trapping on excitation frequency and microsphere diameter

(A–C) (A) LN_100, (B)LN_200, and (C) LN_300 transducers determined experimentally and distribution of effective trapping obtained via calculation of acoustic force in the cases of different frequencies (f) and three sets of particle sizes (d = 2a). (A1–C1) The discriminating factor dFx/dx values of the three focused transducers. (A2–C2) Condition A or B of the three focused transducers calculated by Equation S12, and the gray area represents the forbidden band of acoustic trapping under coordinate system of frequency (f) and ratio (d/λ) ranges. Here, "d" is the diameter of the microsphere, and "λ" is the wavelength of the ultrasound beam at the excitation frequency. Symbol "○" indicates successful trapping, and "×" indicates trapping failure (moving away) in experiments.

trapped particles, and medium (acoustic property of c and ρ), "Forbidden band" could be defined and based on the size-to-wavelength ratio. In this case, the theoretical widths of the "Forbidden band" of three transducers are 1.41 d/λ from 1.01 to 2.42 d/λ, 0.99 d/λ from 1.28 to 2.17 d/λ, and 0.99 d/λ from 1.28 to 2.17 d/λ, respectively. Furthermore, we designed corresponding experiments to verify this theory. All the three $LiNbO_3$ ultrasonic transducers are capable of efficient excitation over a large range of frequencies owing to their high sensitivity and relatively wide bandwidth. In particular, we operate the LN_200 and LN_300 transducers at frequencies of 200–300 MHz and LN_100 transducer at 80–130 MHz. Thus, by modifying the excitation frequency and selecting microspheres with different diameters, we could quantitatively obtain the dependence of trapping effect on excitation frequency and microsphere diameter and compare experimental discrete points with theoretical calculations of the distribution of effective trapping as shown in Figure 4(A2–C2). This shows the dependence of trapping results on the excitation frequency and microsphere diameter to wavelength ratio along with the theoretically calculated frequency (f) and ratio (d/λ) ranges, wherein the gray area indicates that the particles were pushed away, whereas the white area indicates that the particles were trapped. Multiple microspheres are typically trapped simultaneously when $d/\lambda < 0.5$, owing to the beam width and small particle size. However, this case was not considered in current study. As illustrated in Figure 4A, the LN_100 transducer was unable to manipulate microspheres when the particle size-to-wavelength ratio was 1.17–2.48 d/λ, which agrees with the corresponding theoretical range of 1.08–2.49 d/λ. However, the microspheres could be trapped and manipulated via the SBAT at frequencies outside of this range. As shown in Figures 4B and 4C, for the LN_200 and LN_300 transducers, the theoretical range of the particle size-to-wavelength ratio for which particle manipulation was not possible is about 1.28–2.17 d/λ, which is also close to the experimentally obtained range of 1.36–2.34 d/λ and 1.35–2.04 d/λ for the two different transducers, respectively. The forbidden band theory of acoustic radiation force trapping and widths of the forbidden band for all three transducers are little different because they have different center frequencies and *f-number*s. This result indicates that trapping of SBAT is not possible in the range about 1.1 d/λ here the d is the diameter of the target object microsphere and the λ is the wavelength of the medium. This is because a positive gradient of ARF will occur at the focus when the excitation frequency and the size of microsphere achieves nearly 1 d/λ~2 d/λ. Thus, SBATs could be developed for selectively manipulating microspheres of certain sizes by carefully selecting the excitation frequency.

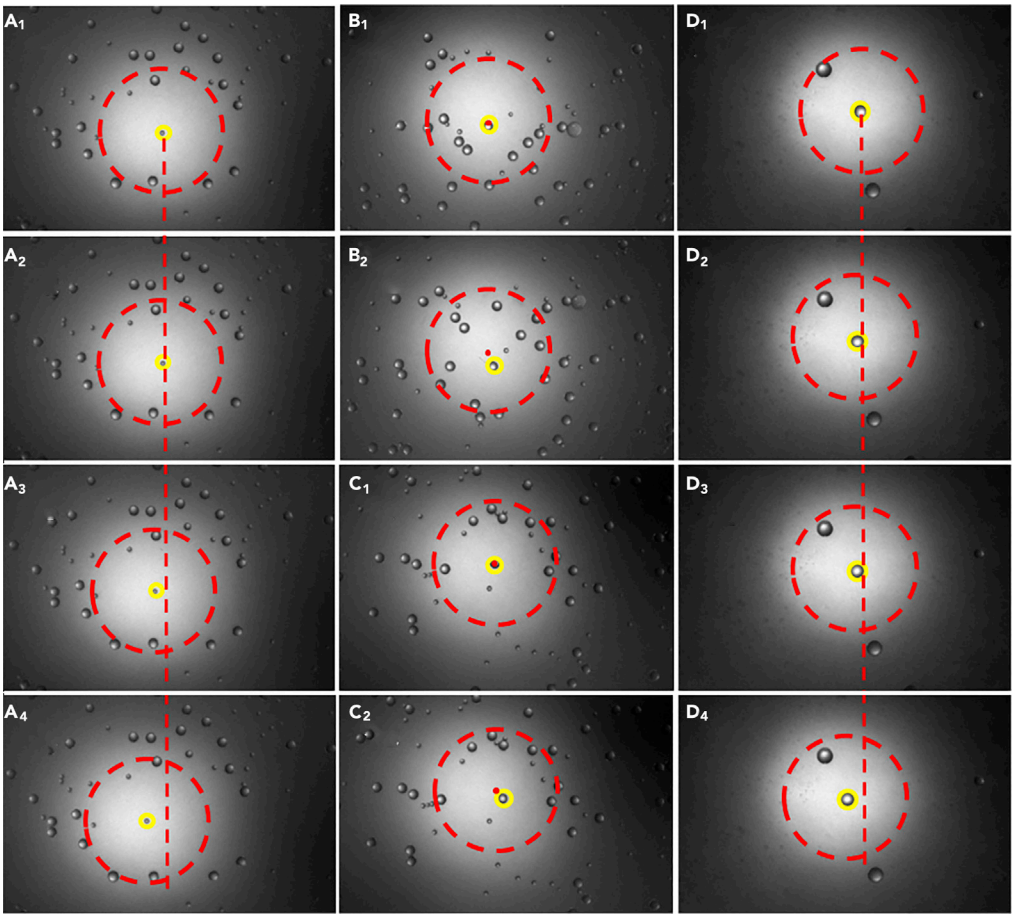

Figure 5. Experiment of size-selective trapping

Examples of manipulation of microspheres of different sizes using the LN_200 transducer. Here, the yellow circles indicate the target microsphere, the red dots or dashed lines depict the location change of the microsphere, and the red dots or the vertical dashed lines are reference points or lines depicting the initial position of the target microsphere and the red circle dotted line represents the position of the transducer.

(A–D) (A) 5-μm microsphere, (B and C) 10-μm microsphere, and (D) 15-μm microsphere. For cases (A and D), the single particle (5 and 15 μm) can be successfully trapped by the LN_200 transducer. However, the 10-μm microsphere moves away and cannot be trapped as shown in cases (B and C).

Selectively manipulating microspheres

The LN_200 transducer was selected for the experimental demonstration to visually depict the size selectivity of SBAT devices; the transducer, was operated at 250 MHz. At 250 MHz, the LN_200 transducer was capable of manipulating a single microsphere with a diameter of 5 or 15 μm; however, it was unable to trap a single microsphere of 10 μm diameter. Figure 5 and Video S1show examples of manipulation of single microspheres of different sizes using this transducer. The bright area with a red circle is the projection of the transducer. Microspheres of three different sizes (5, 10, and 15 μm) were used. The red dashed line or red dot is shown as a reference in Figure 5 to illustrate the position shift of the microspheres. The LN_200 transducer was excited by a sinusoidal burst in different conditions: a driving frequency of 250 MHz; the excitation voltages of 3.6 V, 2.4 V, and 1.2 V for 15, 10, and 5 μm microspheres, respectively; and a duty cycle of 1%. The panels in Figure 5 labeled "A" show the manipulation of a single 5-μm microsphere (yellow circle) that was trapped and manipulated by moving the transducer device. Similarly, the panels labeled "D" are for the 15-μm microsphere. However, for the 10-μm microsphere, the observation was different, in particular, the microsphere moved away from the center of the focus immediately after the transducer was switched on. Our calculation and experimental results provide a deeper understanding of SBATs, which can be used to broaden their applications.

Table 1. The acoustic properties of the cells for trapping

	Cell density (kg/m^3)	Cell compressibility (×10−10 Pa^{-1})	Acoustic impedance (MRayl)
Cell 1	1,000	4.4	1.51
Cell 2	1,210	3.3	1.91

Simulations of radiation force for cells

To estimate the forbidden band in the application of SBAT for cell trapping, the calculations of the force using LN_200 at 250 MHz with different size of cells were performed. As the acoustic properties of the cells are different from the polystyrene spheres used earlier, we chose the two cells with different density and compressibility and the cell size from 5 to 15 μm, which is reported in the literature (Augustsson et al., 2016; Baudoin et al., 2020a, 2020b). Table 1 shows the density and compressibility of two cells (cell 1 and cell 2) with the extreme values. Figures 6A–6C show the simulation of the ARF and ΔF under the two conditions (trapped ΔF > 0 and not trapped ΔF < 0) when the size of cell increasing, where F_1 and F_2 are defined as the extreme value of F_x at $x < 0$ and $x > 0$ and the ΔF is the interpolation of F_1 and F_2. The ΔF of two different cells are shown in Figure 6D, and the white area represents the positive area (trapping) and gray area the negative area (not trapping).

Furthermore, the value of ΔF for two cells is different due to the different acoustic properties, and they all show the same "forbidden band" corresponding to the different sizes (about 7–12 μm). This result demonstrates that the same forbidden band also exists in cells with different acoustic property and constitutes a cornerstone of size selectivity of SBAT for biological applications.

DISCUSSION

In conclusion, size selectivity of SBATs at a cellular level was demonstrated via trapping experiments using tightly focused $LiNbO_3$ transducers with different center frequencies. These transducers are suitable for SBAT applications because they can operate at an ultrahigh frequency and have broad bandwidth, high

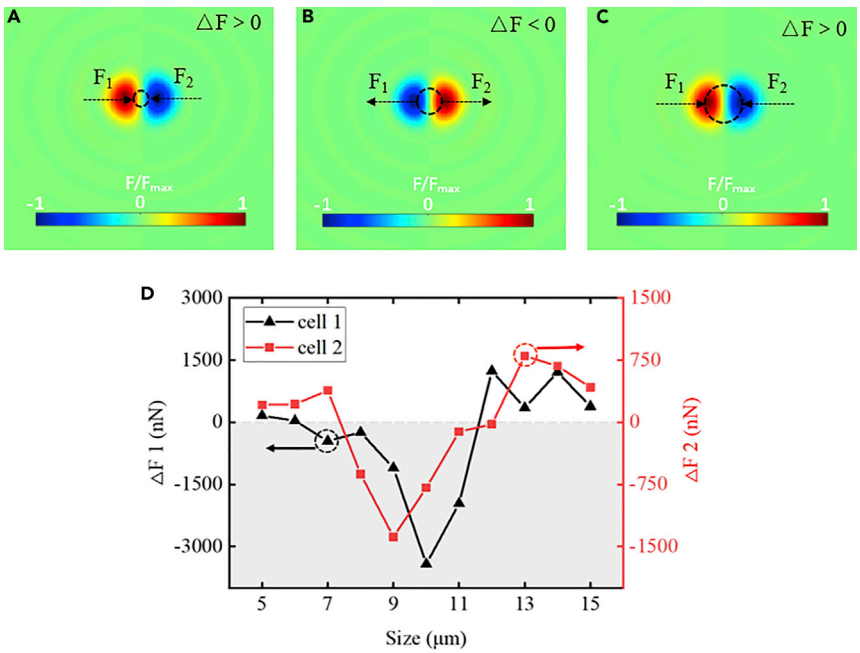

Figure 6. Simulation of the acoustic radiation force of the cell

(A–D) The cell is not trapped (moving away) (ΔF < 0, B, and trapped (ΔF > 0, A and C); the dotted empty circle at the center of the figure represents the cell with different size. The calculation of ΔF for two cells (cell 1 and cell 2) with different sizes from 5 to 15 μm (D).

sensitivity, and small $f_{\#}$. Our experimental trapping results demonstrated that the ratio of particle size-to-wavelength is an important determinant of acoustic trapping. The SBAT devices were found to be capable of selectively manipulating microspheres of certain sizes by adjusting the wavelength of the acoustic beam accordingly; this was, verified via both simulation and theoretical calculation. Additionally, the results are also valid for acoustically trapping cells typically characterized by a lower acoustic contrast compared with polystyrene particles used in the current study and the ARF trapping of live cells in terms of composition, shape, and physical properties would be the next step of our research. These trapping results are promising for the application of SBATs in biomedical and biophysical research. In conclusion, the present work constitutes another important cornerstone toward widespread applications of SBAT for biological and chemical research applications.

Limitations of the study

This study presents the dependency of trapping capability of high-frequency focused ultrasonic beam on the working frequency and particle diameter, which is useful in the selective manipulation of cells and other small particles. Two main limitations are as follows: (1) The particles trapped in the article are spheres or ellipsoids so that they can be substituted into Equations (1) and (2) to calculate the acoustic radiation force. If the particles have irregular shapes, you need to use the FEM to model and simulate the incident sound field and its scattering field and calculate the sound radiation force by integrating the sound field. (2) The trapped particles selected for the experiment in the article are PDMS, which is uniform and not easy to deform. Suppose the "Forbidden Band" effects are used to manipulate real cells. In that case, it is essential to characterize the material's acoustic and mechanical properties and then substitute it into the formula. More importantly, the cell's deformation also needs to be considered because this affects the distribution of the scattered field and the direction and magnitude of the final force will change. It is also necessary to perform accurate sound field analysis on the focusing transducer used as acoustic tweezers. If the frequency ($\geq$100 MHz) is too high (in this article), the sound field distribution can only be obtained by FEM, not by an experimental hydrophone test.

Resource availability

Lead contact

Further information and requests for resources and reagents should be directed to and will be fulfilled by the Lead Contact, Prof. Chunlong Fei (clfei@xidian.edu.cn).

Materials availability

This study did not generate new unique materials.

Data and code availability

All data associated with the study are included in the paper.

METHODS

All methods can be found in the accompanying Transparent methods supplemental file.

SUPPLEMENTAL INFORMATION

Supplemental information can be found online at https://doi.org/10.1016/j.isci.2020.101988.

ACKNOWLEDGMENTS

Financial support from the National Natural Science Foundation of China of China (No: 61974110), the Natural Science Foundations of Shaanxi Province (No: 2020JM-205), the Shaanxi Provincial Association of Science and Technology Young Talents Support Project (No: 20190105), Shenzhen Science technology and fundamental research and discipline layout project (No: JCYJ20170818153048647), and the National Key Research and Development Program of China (No: 2017YFC0109703) are greatly appreciated.

AUTHOR CONTRIBUTIONS

Conceptualization, C.F. and Y.Y.; Methodology, Z.L., D.W., Z.Q., and D.C.; Investigation, D.L., Q.Z., and Z.C.; Software, Z.L., R.W., and C.H.; Writing – Original Draft, Z.L., D.W., and C.F.; Writing – Review & Editing, Z.L., C.F., Z.Q., and D.W.; Supervision, C.F.; Funding Acquisition, C.F. and Y.Y.

DECLARATION OF INTERESTS

The authors declare no competing interests.

Received: October 14, 2020
Revised: November 22, 2020
Accepted: December 18, 2020
Published: January 22, 2021

REFERENCES

Ashkin, A., Dziedzic, J., Bjorkholm, J., and Chu, S. (1986). Observation of a single-beam gradient force optical trap for dielectric particles. Opt. Lett. *11*, 288.

Augustsson, P., Karlsen, J., Su, H., Bruus, H., and Voldman, J. (2016). Iso-acoustic focusing of cells for size-insensitive acousto-mechanical phenotyping. Nat. Commun. *7*, 1–9.

Baudoin, M., Thomas, J., Sahely, R., Gerbedoen, J., Gong, Z., Sivery, A., Matar, O., Smagin, N., Favreau, P., and Vlandas, A. (2020a). Spatially selective manipulation of cells with single-beam acoustical tweezers. Nat. Commun. *11*, 4244.

Baudoin, M., Thomas, J., Sahely, R., Gerbedoen, J., Gong, Z., Sivery, A., Matar, O., Smagin, N., Favreau, P., and Vlandas, A. (2020b). Spatially selective manipulation of cells with single-beam acoustical tweezers. Nat. Commun. *11*, 1–10.

Chen, X., Lam, K., Chen, R., Chen, Z., Yu, P., Chen, Z., Shung, K., and Zhou, Q. (2017). An adjustable multi-scale single beam acoustic tweezers based on ultrahigh frequency ultrasonic transducer. Biotechnol. Bioeng. *114*, 2637–2647.

Choe, Y., Kim, J., Shung, K., and Kim, E. (2011). Microparticle trapping in an ultrasonic Bessel beam. Appl. Phys. Lett. *99*, 233704.

Diamantaki, M., Coletta, S., Nasr, K., Zeraati, R., Laturnus, S., Berens, P., Preston-Ferrer, P., and Burgalossi, A. (2018). Manipulating hippocampal place cell activity by single-cell stimulation in freely moving mice. Cell Rep. *23*, 32–38.

Fazal, F., and Block, S. (2011). Optical tweezers study life under tension. Nat. Photon. *5*, 318–321.

Grier, D. (2003). A revolution in optical manipulation. Nature *424*, 810–816.

Kamsma, D., Bochet, P., Oswald, F., Alblas, N., Goyard, S., Wuite, G., Peterman, E., and Rose, T. (2018). Single-cell acoustic force spectroscopy: resolving kinetics and strength of T cell adhesion to fibronectin. Cell Rep. *24*, 3008–3016.

Keloth, A., Anderson, O., Risbridger, D., and Paterson, L. (2018). Single cell isolation using optical tweezers. Micromachines *9*, 434.

Kirkham, G., Britchford, E., Upton, T., Ware, J., Gibson, G., Devaud, Y., Ehrbar, M., Padgett, M., Allen, S., Buttery, L., et al. (2015). Precision assembly of complex cellular microenvironments using holographic optical tweezers. Sci. Rep. *5*, 1–7.

Kotamarthi, H., Sauer, R., and Baker, T. (2020). The non-dominant AAA+ ring in the ClpAP protease functions as an anti-stalling motor to accelerate protein unfolding and translocation. Cell Rep. *30*, 2644–2654.e3.

Lam, K., Hsu, H., Li, Y., Lee, C., Lin, A., Zhou, Q., Kim, E., and Shung, K. (2012). Ultrahigh frequency lensless ultrasonic transducers for acoustic tweezers application. Biotechnol. Bioeng. *110*, 881–886.

Lee, J., and Shung, K. (2006). Effect of ultrasonic attenuation on the feasibility of acoustic tweezers. Ultrasound Med. Biol. *32*, 1575–1583.

Lee, J., Ha, K., and Shung, K. (2005). A theoretical study of the feasibility of acoustical tweezers: ray acoustics approach. The J. Acoust. Soc. America *117*, 3273–3280.

Lee, J., Teh, S., Lee, A., Kim, H., Lee, C., and Shung, K. (2009). Single beam acoustic trapping. Appl. Phys. Lett. *95*, 073701.

Lee, J., Lee, C., Kim, H., Jakob, A., Lemor, R., Teh, S., Lee, A., and Shung, K. (2011). Targeted cell immobilization by ultrasound microbeam. Biotechnol. Bioeng. *108*, 1643–1650.

Liu, Y., and Hu, J. (2009). Ultrasonic trapping of small particles by a vibrating rod. IEEE Trans. Ultrason. Ferroelectr. Freq. Control *56*, 798–805.

Maragò, O., Jones, P., Gucciardi, P., Volpe, G., and Ferrari, A. (2013). Optical trapping and manipulation of nanostructures. Nat. Nanotechnol. *8*, 807–819.

Marston, P. (2006). Axial radiation force of a Bessel beam on a sphere and direction reversal of the force. J. Acoust. Soc. Am. *120*, 3518–3524.

Melde, K., Mark, A., Qiu, T., and Fischer, P. (2016). Holograms for acoustics. Nature *537*, 518–522.

Neuman, K., and Nagy, A. (2008). Single-molecule force spectroscopy: optical tweezers, magnetic tweezers and atomic force microscopy. Nat. Methods *5*, 491–505.

Ozcelik, A., Rufo, J., Guo, F., Gu, Y., Li, P., Lata, J., and Huang, T. (2018). Acoustic tweezers for the life sciences. Nat. Methods *15*, 1021–1028.

Padgett, M., and Bowman, R. (2011). Tweezers with a twist. Nat. Photon. *5*, 343–348.

Patnode, M., Beller, Z., Han, N., Cheng, J., Peters, S., Terrapon, N., Henrissat, B., Le Gall, S., Saulnier, L., Hayashi, D., et al. (2019). Interspecies competition impacts targeted manipulation of human gut bacteria by fiber-derived glycans. Cell *179*, 59–73.e13.

Quinto-Su, P. (2014). A microscopic steam engine implemented in an optical tweezer. Nat. Commun. *5*, 1–7.

Sitters, G., Kamsma, D., Thalhammer, G., Ritsch-Marte, M., Peterman, E., and Wuite, G. (2014). Acoustic force spectroscopy. Nat. Methods *12*, 47–50.

Tomasi, R., Sart, S., Champetier, T., and Baroud, C. (2020). Individual control and Quantification of 3D spheroids in a high-density microfluidic droplet array. Cell Rep. *31*, 107670.

Wu, J. (1991). Acoustical tweezers. J. Acoust. Soc. Am. *89*, 2140–2143.

Yu, Y., and Miyako, E. (2018). Alternating-Magnetic-field-mediated wireless manipulations of a liquid metal for therapeutic bioengineering. Iscience *3*, 134–148.

Zhu, B., Xu, J., Li, Y., Wang, T., Xiong, K., Lee, C., Yang, X., Shiiba, M., Takeuchi, S., Zhou, Q., et al. (2016). Micro-particle manipulation by single beam acoustic tweezers based on hydrothermal PZT thick film. AIP Adv. *6*, 035102.

iScience, Volume *24*

Supplemental Information

The forbidden band and size selectivity of acoustic radiation force trapping

Zhaoxi Li, Danfeng Wang, Chunlong Fei, Zhihai Qiu, Chenxue Hou, Runcong Wu, Di Li, Qidong Zhang, Dongdong Chen, Zeyu Chen, Wei Feng, and Yintang Yang

Supplemental material files: The Forbidden Band and Size Selectivity of Acoustic Radiation Force Trapping

Zhaoxi Li[1#], Danfeng Wang[2#], Chunlong Fei,[1,5,], Zhihai Qiu[3], Chenxue Hou[1], Runcong Wu[1], Di Li[1], Qidong Zhang[1], Dongdong Chen[1], Zeyu Chen[2], Wei Feng[4], Yintang Yang[1,*]*

[1] School of Microelectronics, Xidian University, Xi'an, China

[2] School of Mechanical and Electrical Engineering, Central South University, Changsha, China

[3] Department of Radiology, Stanford University, Stanford, CA, US

[4] Shenzhen Institutes of Advanced Technology, Chinese Academy of Sciences, 518055, China

[5] Lead contact

Transparent Methods

Calculation of acoustic radiation force

Based on the theoretical calculation for acoustic radiation force (ARF) calculations on nonabsorbent spherical scatterer placed in an ideal fluid, the first proposed radiation force **F** on a small sphere in an acoustic field with an arbitrary structure could be described as F =-∇U and the potential U is the Gor'kov (Gor'kov, 1962) potential, which can be represented as follows:

$$U = \frac{\pi a^3}{3}\left\{f_1 \frac{|p|^2}{\rho c^2} - \frac{3}{2} f_2 \rho |\mathbf{v}|^2\right\} \tag{3}$$

$$f_1 = 1 - \frac{\rho c^2}{\rho_* c_l^2} \frac{1}{1 - \frac{4c_t^2}{3c_l^2}} \tag{4}$$

$$f_2 = 2\frac{\rho_* - \rho}{2\rho_* + \rho} \tag{5}$$

where a is the radius of the spherical particle; ρ_* is its density; c_l and c_t are longitudinal wave velocity and shear wave velocity in the material of the particle, respectively; c is the fluid sound velocity and ρ is density of the fluid; p is the acoustic pressure distribution at the target plane and $\mathbf{v}$ is particle velocity in the fluid, respectively. This algorithm simply gives the magnitude and direction of the acoustic radiation force (F) at a certain position, when the sound field distribution (p and $\mathbf{v}$) of th position and the acoustic characteristics of particle and liquid are given. For very small sphere as scatterers in the diffraction acoustic field, just the monopole and dipole terms need to be considered in the calculation of acoustic field and acoustic radiation force which is called the Rayleigh scattering regime (Harada and Asakura, 1996). However, the abovementioned expression is valid only for a microsphere or ellipsoid with the diameter that is significantly smaller than the acoustic wavelength. The size-to-wavelength ratio covered within this work is at the upper limit or even beyond the Rayleigh regime. Furthermore, the angular spectrum using the Fourier transform of the scattered field formed by all incident acoustic waves can be superimposed to express the net scattered field. In particular, Sapozhnikova (Sapozhnikov and Bailey, 2013) developed a theoretical approach that calculates the radiation force of the elastic sphere in the arbitrary acoustic beam without a size limitation, the components of the radiation force (viz. F_x, F_y, and F_z) can be given by:

$$F_x = \frac{1}{8\pi^2\rho c^2 k^2} Re\left\{\sum_{n=0}^{\infty} \psi_n \sum_{m=-n}^{n} A_{nm}\left(H_{nm}H_{n+1,m+1}^{*} - H_{n,-m}H_{n+1,-m-1}^{*}\right)\right\} \tag{6}$$

$$F_y = \frac{1}{8\pi^2\rho c^2 k^2} Im\left\{\sum_{n=0}^{\infty}\psi_n \sum_{m=-n}^{n} A_{nm}\left(H_{nm}H_{n+1,m+1}^{*} + H_{n,-m}H_{n+1,-m-1}^{*}\right)\right\} \tag{7}$$

$$F_z = -\frac{1}{4\pi^2\rho c^2 k^2} Re\left\{\sum_{n=0}^{\infty}\psi_n \sum_{m=-n}^{n} B_{nm}H_{nm}H_{n+1,m}^{*}\right\} \tag{8}$$

where function $H_{nm} = \iint_{k_x^2+k_y^2\le k^2} dk_x dk_y S(k_x,k_y) Y_{nm}^{*}(\theta_k,\varphi_k)$ and the $S(k_x,k_y)$ is the angular spectrum of the acoustic wave generated via transducer, k is the wavenumber in the fluid, φ_k is the polar angles and θ_k is the spherical angle of the wave vector of the wave vector $\boldsymbol{k} = \left\{k_x, k_y, \left(k^2 - k_x^2 - k_y^2\right)^{1/2}\right\}$, respectively, c is sound velocity of the fluid, functions $Y_{nm}(\theta_k,\varphi_k)$ represent spherical harmonics, $A_{nm} = \sqrt{(n+m+1)(n+m+2)/(2n+1)(2n+3)}$ and $B_{nm} = \sqrt{(n+m+1)(n-m+1)/(2n+1)(2n+3)}$. The ψ_n can be obtained from the equation $\psi_n = 2(c_n + c_{n+1}^{*} + 2c_n c_n^{*})$ and the (*) represents the complex conjugation. The scattering coefficients c_n are determined by Eqs. (S1-S4) in III Supplemental Material.

It should be noted that the angular spectrum of the beam $S(k_x,k_y)$ is obtained based on the distribution of complex acoustic pressure $p(x,y,z_0)$ generated by the transducer in the focal plane($z=z_0$):

$$S(k_x,k_y) = \iint_{-\infty}^{+\infty} p(x,y,z_0)\, e^{-ik_x x - ik_y y} dxdy \tag{9}$$

Through the above formulas, we can respectively calculate the three components of acoustic radiation force (F_x, F_y and F_z) when the acoustic characteristics of the propagation medium (ρ and c) and the scatterer (c_l, c_t, a and ρ_*) and complex sound field distribution

$p(x, y, z_0)$ are known. It should be noted that the position of the initial scatterer is at the origin of the coordinate system (x,y,z)=(0,0,0) and the specific factor given in II Supplemental Material is multiplied by the angular spectrum for calculating the acoustic radiation force in any area. Therefore, acoustic force on a trapped elastic sphere can be calculated when the magnitude and phase of acoustic pressure is obtained using hydrophone scanning or bia finite element method (FEM) analysis on the plane of interest.

Materials and Preparation

Tightly focused LiNbO3 transducers with center frequency around 100MHz (LN100), 200MHz (LN200) and 300MHz (LN300) were designed and fabricated, respectively. The fabrication and characterization details were described previously (Fei et al., 2016; Cannata et al., 2003).

The microspheres trapping experiments were conducted in a filling distilled water cell culture dish with the focused needle ultrasound transducer. The needle transducer was manipulated by the three-axis motorized linear stage (LMG26 T50 MM, OptoSigma, CA) using LabVIEW program. Photographs and movies of the capture and movement of the microspheres were acquired by a CMOS camera (ORCA-Flash 2.8, Hamamatsu, Japan) combined with an inverted microscope (IX-71, Olympus, Japan) under the cell culture dish.

To perform microspheres manipulation. A function generator (SG384 Stanford Research System, CA) provides the reference signal in a sinusoidal burst mode and a 50 dB power low impedance amplifier (525 LA, ENI Rochester, MN) directly drives the transducers with designed repetition frequency of the pulse, peak-to-peak magnitude of voltage and duty cycle corresponding to pulse.

Trapping experiment

For the particle trapping experiment of Size-selectivity several kinds of particle are immersed inside the cell. It is made from Polystyrene microspheres (Microbead NIST traceable particle size standard, Polyscience, Inc., Warrington, PA) with different diameters. The longitudinal sound velocity of the polystyrene material used to make the microspheres is 2330 m/s, the transverse sound velocity is 1100 m/s, and the density is 1040 kg/m^3. Firstly, the transducer is manipulated perpendicularly to the beam axis at the focal distance where the single microsphere is located. Immediately when the transducer is excited by the signal, there will form an acoustic trap at the focal distance if the microsphere size is suitable for trapping, otherwise the microsphere will move away from the center of the focus. Polystyrene microspheres of 5 μm, 10 μm, 15 μm, and 45 μm diameter were chosen as the targets.

Transducer characterization

The mathematical function with f-number ($f_{\#}$) of the focus transducer can be expressed as:

$$f_{\#} = \frac{L_{DOF}}{D}$$

Where L_{DOF} and D are the depth of the focus and the diameter of the focused transducer, respectively. In order to achieve lower f-number ($\leqslant 1$) and high sound pressure intensity, smaller focal length is required when the transducer has been made.

The -6dB bandwidth can be described by:

$$BW = \frac{f_{upper} - f_{lower}}{f_c}$$

$$f_c = \frac{f_{lower} + f_{upper}}{2}$$

Where f_c is the center frequency of the transducer. f_{lower} and f_{upper} are the lower frequency and upper frequency of the bandwidth of −6dB points in receive-echo frequency spectrum. The broad − 6 dB bandwidth (> 30%) shows a wide range of operating frequency for trapping.

Equations of ARF calculation:

$$c_n = -\frac{\Gamma_n j_n(ka) - kaj_n'(ka)}{\Gamma_n h_n^{(1)}(ka) - kah_n^{(1)'}(ka)}, \quad \Gamma_n = \frac{\rho k_t^2 a^2}{2\rho_s}\frac{\alpha_n\delta_n + \beta_n\chi_n}{\alpha_n\eta_n + \beta_n\varepsilon_n}, \tag{S1}$$

$$\alpha_n = j_n(k_l a) - k_l a j_n'(k_l a), \quad \beta_n = (n^2 + n - 2)j_n(k_t a) + k_t^2 a^2 j_n''(k_t a) \tag{S2}$$

$$\chi_n = k_l a j_n'(k_l a), \quad \delta_n = 2n(n+1)j_n(k_t a), \quad \varepsilon_n = k_l^2 a^2\left[\frac{j_n(k_t a)\sigma}{1-2\sigma} - k_l a j_n''(k_l a)\right], \tag{S3}$$

$$\eta_n = 2n(n+1)[j_n(k_t a) - k_t a j_n'(k_t a)], \quad \sigma = (c_l^2/2 - c_t^2)/(c_l^2 - c_t^2), \tag{S4}$$

where $j_n(\cdot)$ is the spherical Bessel functions and $h_n^{(1)}(\cdot)$ is the first kind spherical Hankel functions of ; here ,a prime (') represents differentiation pertaining to the argument; the value of n is a natural number; $k_l = 2\pi f/c_l$ and $k_t = 2\pi f/c_t$ are the wavenumbers of longitudinal and shear waves in the material of the sphere respectively and a is the radius of the sphere.

Supplementary Figures

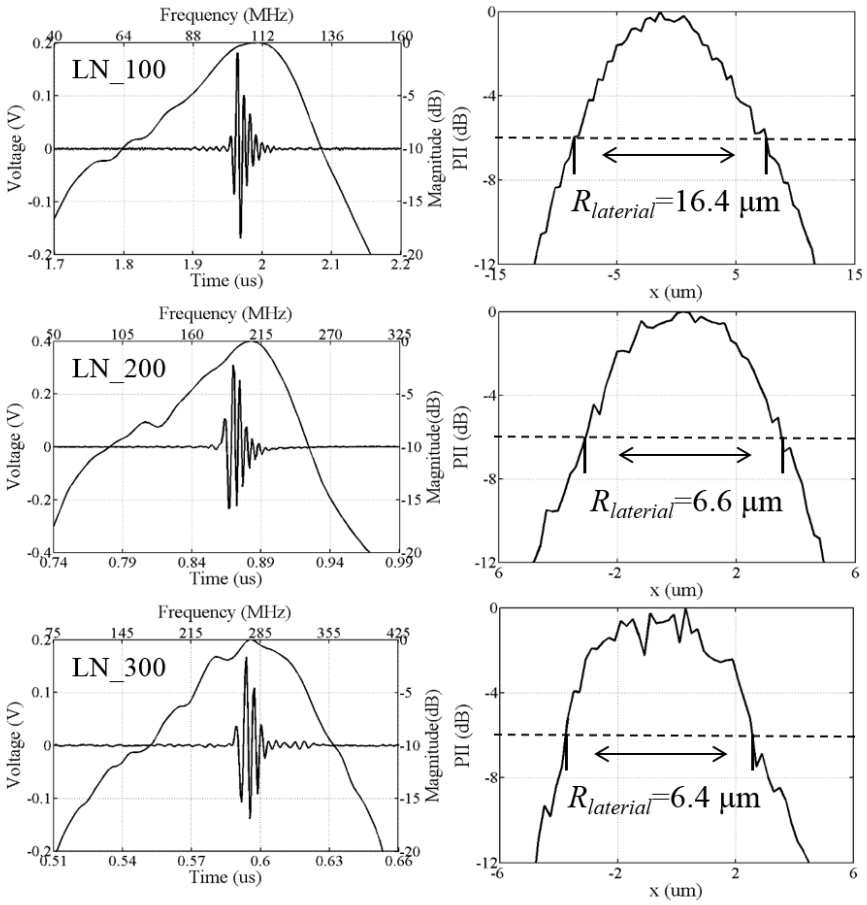

Fig.S1 [The characterization of three transducers. (related to Figure 1).] Time-domain pulse/echo response and frequency spectrum (left) as well as lateral beam profile (right) of the transducers.

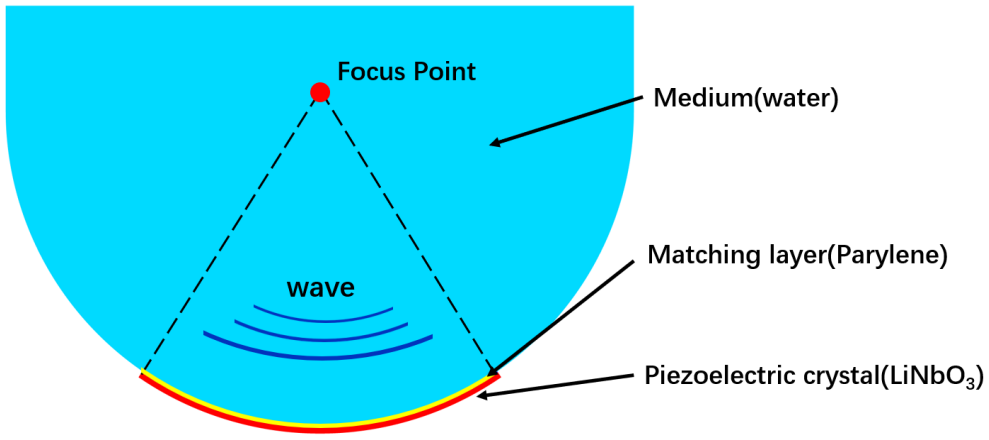

Fig.S2. [The FEM model of focused transducer (related to Figure 2).] The model consisted of Matching layer (Parylene), ball-press piezoelectric transducers ($LiNbO_3$), and water. Utilizing the solid

mechanics and electrostatics modules in combination with a piezoelectric multiphysics coupling, we were able to apply oscillatory voltages to the transducers and explore the sound field. The boundaries at the ends of the water (covered with tape) were modelled as low-reflecting boundaries and between Matching layer and piezoelectric crystal is Acoustic-Structure Boundary multiphysics coupling.

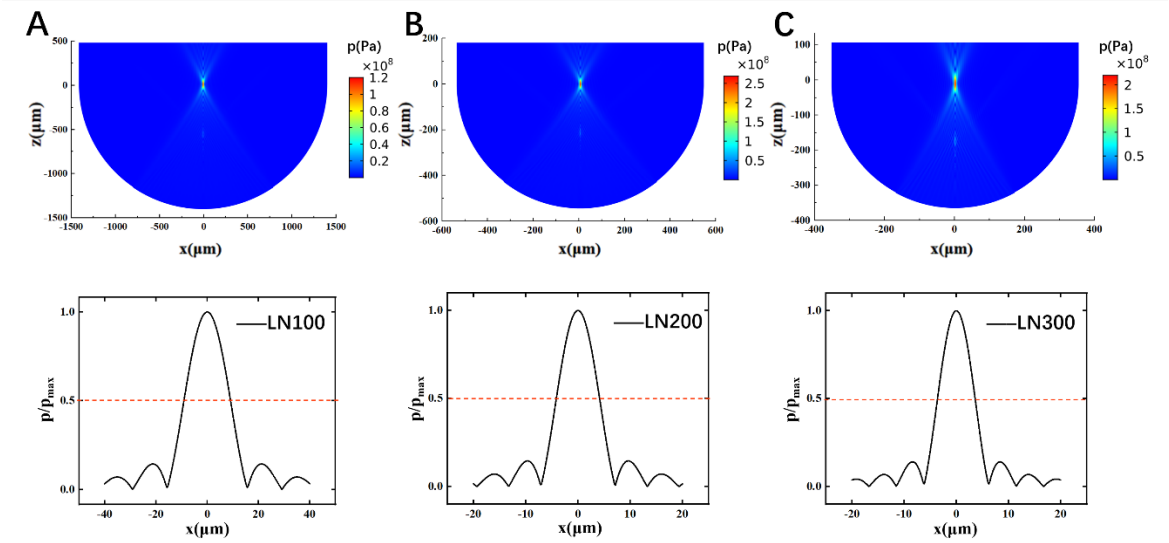

Fig.S3. [Magnitudes for the different frequency spectral component of the fields produced with three ball-press needle transducer (related to Figure 2).] Comparison of the magnitude of the FEM data at their working frequency, taken through the center of focus for each transducer (A) LN100 (B) LN200 (C)LN300 at 100 MHz , 200MHz and 300MHz respectively.

Supplementary Tables

Table.S1 [Summary of transducers performance. (related to Figure 1)]

	LN_100	LN_200	LN_300
f_c (MHz)	104	207	275
BW (%)	40.3	44.2	45.05
IL (dB)	18.8	21.5	28.8
$f_{\#}$	0.84	0.83	1.15
$R_{lateral}$ (μm)	16.4	6.6	6.4

Supplemental References

Gor'kov, L. P. (1962). On the forces acting on a small particle in an acoustical field in an ideal fluid. In Sov. Phys. Dokl. *6* 773-775.

Harada, Y., and Asakura, T. (1996). Radiation forces on a dielectric sphere in the Rayleigh scattering regime. Optics Communications *124*, 529-541.

Sapozhnikov, O., and Bailey, M. (2013). Radiation force of an arbitrary acoustic beam on an elastic sphere in a fluid. The Journal Of The Acoustical Society Of America *133*, 661-676.

Fei, C., Chiu, C., Chen, X., Chen, Z., Ma, J., Zhu, B., Shung, K., and Zhou, Q. (2016). Ultrahigh Frequency (100 MHz–300 MHz) Ultrasonic Transducers for Optical Resolution Medical Imagining. Scientific Reports *6,* 1-8.

Cannata, J., Ritter, T., Wo-Hsing Chen, Silverman, R., and Shung, K. (2003). Design of efficient, broadband single-element (20-80 MHz) ultrasonic transducers for medical imaging applications. IEEE Transactions On Ultrasonics, Ferroelectrics And Frequency Control *50*, 1548-1557.